Polymer Composites

WILEY | spe INSPIRING PLASTICS PROFESSIONALS

RESEARCH ARTICLE OPEN ACCESS

Improved Flexural Properties of Carbon Fiber-Reinforced Polyamide Composites for Type IV and V Hydrogen Storage Vessels Utilizing Graphene Nanoplatelets

Jonghyun Eun[1] | Sun-Woo Kang[2,3] | Myeongjin Park[1] | Joon Seok Lee[3] | Hyunchul Ahn[3]

[1]Department of Materials Design Engineering, Kumoh National Institute of Technology, Gumi, Republic of Korea | [2]SpacePro, Miryang, Republic of Korea | [3]Department of Fiber System Engineering, College of Engineering, Yeungnam University, Gyeongsan, Republic of Korea

Correspondence: Joon Seok Lee (leejs@ynu.ac.kr) | Hyunchul Ahn (hyunchul.ahn@yu.ac.kr)

Received: 4 August 2025 | **Revised:** 9 October 2025 | **Accepted:** 11 October 2025

Funding: This study was supported by the Technology Innovation Program (20011899) funded by the Ministry of Trade, Industry & Energy (MOTIE, Korea) and supported by the 2023 Yeungnam University Research Grant.

Keywords: carbon fiber-reinforced composites | graphene nanoplatelets | hydrogen storage vessel | polyamide

ABSTRACT

This study explores the enhancement of bending properties in carbon fiber-reinforced polyamide6 (PA6) composites for Type IV and V hydrogen storage vessels through the incorporation of graphene nanoplatelets (GNPs). PA6 materials, widely utilized as liner materials in such applications, require superior flexural properties and impact resistance to withstand the demands of pressure vessels. By integrating GNPs, it is aimed to improve these mechanical properties without compromising the resin's hydrogen barrier capabilities and moldability. The results revealed that the flexural strength and modulus of PA6-based composites were significantly improved by the addition of GNPs, with 0.6 wt% identified as the optimal loading. At this composition, a well-dispersed GNPs network acted as an effective nucleating agent, enhancing crystallinity, stress transfer, and interfacial adhesion, thereby achieving the best overall mechanical performance. In contrast, lower or higher GNPs loadings led to inferior reinforcement due to insufficient network formation or agglomeration. These improvements directly support the adaptability of the composites to hydrogen storage vessels, as superior flexural properties are crucial for withstanding high-pressure operating conditions. Through comprehensive evaluation of the resin's properties, the optimal composition was determined, and subsequent fabrication and testing of the composites confirmed their suitability for Type IV and potential application in Type V hydrogen storage vessels.

1 | Introduction

Hydrogen is widely recognized as a promising energy carrier for achieving a zero-carbon future, with applications in transportation, stationary power, and grid energy storage. The safe and efficient storage of hydrogen is a critical technological challenge, particularly for high-pressure applications such as fuel cell vehicles and portable energy systems. Hydrogen storage containers are divided into Types I–V depending on their type, and currently III or IV are mainly used. Type III uses a metal liner and is currently the most widely used, but type IV, which uses a polymer liner to complement the weaknesses of metal materials such as hydrogen embrittlement, is being studied the most and is in the process of conquering the market [1]. Type V hydrogen storage containers are composite containers in which the resin also functions as a liner, breaking away from the existing structure

Jonghyun Eun and Sun-Woo Kang contributed equally to this work.

Summary

- Graphene nanoplatelets enhanced polyamide6 resin's properties.
- The best performance occurred at 0.6 wt% in this research.
- At optimum condition, flexural strength improved more than 27%.
- Thermal characteristics also improved for composite vessel processing.
- Enables over 20% weight cut for ultralight hydrogen storage vessels.

of manufacturing the liner separately, so that the composite container itself can function as a liner. Since there are many advantages such as economy, efficiency, and storage capacity due to the absence of a liner, it is being studied as a next-generation structure [2, 3]. In particular, for hydrogen storage containers that prioritize weight reduction and efficiency, such as those for vehicles, the development of type IV or V is necessary. Hydrogen storage vessels, also known as pressure cylinders or tanks, are engineered to contain hydrogen gas at pressures typically ranging from 350 to 700 bar, necessitating advanced materials and design strategies to ensure both safety and performance [4]. Type IV vessels, which are currently the industry standard for automotive applications, feature a polymer liner—commonly high-density polyethylene (HDPE) or polyamide (PA)—fully wrapped with carbon fiber-reinforced polymer composites (CFRPs) [5] or glass fiber reinforced composites [6].

The choice of liner material is crucial for minimizing hydrogen permeation and ensuring vessel durability. Although metallic liners are robust, they are heavy and susceptible to hydrogen embrittlement. Polymeric liners, such as HDPE and PA, offer significant weight savings and improved chemical resistance. Notably, polyamide liners have demonstrated superior hydrogen barrier properties—up to 30% higher than metals and 50% higher than HDPE—along with a weight reduction of 50%–70% compared to traditional materials [7, 8]. These advantages have driven the adoption of PA as a liner material in next-generation Type IV hydrogen vessels.

Type IV hydrogen storage vessels, with their lightweight polymer liners and CFRPs overwraps, have become the preferred solution for high-pressure storage in automotive and portable applications. However, the long-term performance of these vessels is challenged by hydrogen permeation through the polymer liner and potential degradation of mechanical properties under cyclic loading [9] and temperature changes [10]. Research efforts have therefore focused on improving the barrier and mechanical properties of both the liner and the composite shell [11]. To further enhance the performance of polymer liners and matrix resins, the incorporation of nanomaterial additives has emerged as a promising strategy [12]. Among these, graphene nanoplatelets (GNPs) have attracted significant attention due to their exceptional mechanical strength, high aspect ratio, and impermeability to gases. The addition of GNPs to polyamide matrices has been shown to significantly improve both the mechanical properties and hydrogen barrier performance of the resulting composites [13, 14]. For example, recent studies have reported up to an 83% reduction in hydrogen permeability and notable increases in impact resistance with the inclusion of GNPs in polyamide liners [15]. The mechanism underlying these improvements is attributed to the increased tortuosity of diffusion pathways and enhanced interfacial adhesion between the nanofillers and polymer matrix [16]. Other advanced fillers, such as reduced graphene oxide [17], MXenes [18], carbon nanotubes [19], and nanoclays [20], are also being explored for their potential to further improve the safety and durability of hydrogen storage vessels. In reinforced resins, including those containing GNPs, it was observed improvements in impact strength [21] and fatigue performance [22] those properties critical for high-pressure vessels subjected to cyclic loading. Notably, GNPs addition yielded marked enhancements in microstructural refinement [23] and interfacial properties [24, 25] essential for application in high-pressure hydrogen vessels. Additionally, the development of recyclable thermoplastic resins offers new opportunities for sustainable and high-performance composite tanks [26].

In this study, it was investigated the properties of carbon fiber-reinforced composite structures utilizing polyamide 6 (PA6) materials, which are commonly used as liner materials for Type IV or V applications. Given the characteristics of fiber-reinforced composites for pressure vessels, flexural properties and impact resistance are crucial. To enhance these properties without compromising the hydrogen barrier properties and moldability of the resin, graphene nanoparticles were incorporated. We evaluated the properties of graphene-enhanced PA resin and the carbon fiber-reinforced composites made from this resin, assessing their potential use as hydrogen storage vessels. By evaluating the resin's properties, we identified the optimal composition and confirmed its applicability for hydrogen storage vessels. Furthermore, we manufactured composites using this resin and, through flexural and impact testing, verified their suitability for use in Type IV, and potentially Type V, hydrogen storage vessels (Figure 1).

2 | Materials and Methods

2.1 | Materials

The resin used in this study is PA6 (Grilamid L 25A NZ, EMS Griltech, Domat/EMS, Switzerland), which is widely utilized as a liner material due to its hydrogen barrier properties and moldability. The graphene nanoplatelets (GNPs) used as additives were from Sigma Aldrich (Burlington, Massachusetts, U.S.). The EA used to prepare the PA6 solution was 99.4%, also procured from Sigma Aldrich. The carbon fiber fabric was supplied by Hankuk Advanced Materials (Gwangju, Korea) and was made from T-700 grade carbon fibers. Tables 1 and 2 summarize the detailed specifications of PA6, Carbon fiber, GNPs, and EA.

2.2 | Manufacturing Methods

The PA6 solution was prepared to impregnate the layered fabric, with a controlled weight ratio of PA6, EA, and water

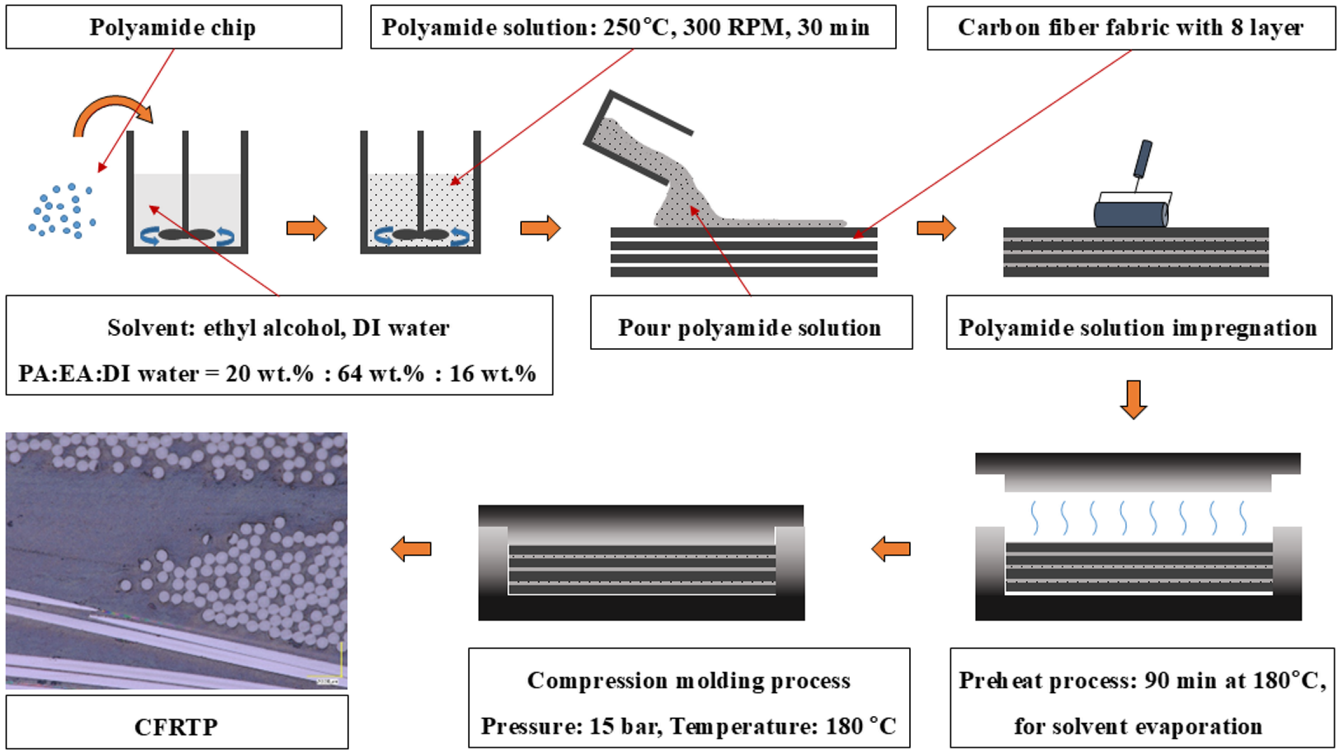

FIGURE 1 | Preparation process of the polyamide solution and compression molding process of carbon fiber reinforced thermoplastic composites.

TABLE 1 | Detailed specifications of PA6, carbon fiber.

	PA6	Carbon fiber
Tensile strength	—	4.9 GPa
Yield stress	30 MPa	
Tensile modulus	750 MPa	230 GPa
Density	840 kg/m^3	1.8 g/cm^3
Elongation at break	> 50%	2.0%
Melting temperature (theoretical)	178°C	

TABLE 2 | Detailed specifications of GNPs, and EA.

	GNPs	EA
Surface area	120–150 m^2/g	—
Particle size	5 μm	—
Bulk density	0.03–0.1 g/cm^3	—
Molecular weight	12.01 g/mol	46.07 g/mol
Thickness	12 nm	—

at 20 wt%: 64 wt%: 16 wt%. This solution underwent a meticulous stirring process at 300 RPM for 30 min on the heated plate maintained at 250°C. The carbon fiber composites were fabricated based on this PA6 solution made by each batch containing GNPs. The fabrication process involved a precise preheating stage at 180°C for 90 min. Subsequently, the preheated fabric was subjected to controlled pressing at 180°C under a pressure of 15 bar, ensuring stringent adherence to engineering specifications and manufacturing precision. In addition, in order to compare the properties of PA6 composite materials, composite samples using PA6 films were produced under the same conditions using film insert molding, and the resin transfer and resin impregnation behaviors were compared. The GNPs-reinforced resin was applied at 0.3, 0.6, and 0.9 wt% to ensure stable dispersion of GNPs, and CFRPs were manufactured using the resin. In addition, the composite manufacturing process variables utilized the stabilized molding conditions of in the previous study [27].

2.3 | Experimental

The micro-structure of the CFRPs were investigated by optical microscope (VHX-S750E, Keyence Co., Osaka, Japan) for investigating interface of CFRPs. The rheological analysis of all the materials was done using a MCR 302e rheometer (Anton Paar, Graz, Austria). The temperature used in the rheometer was 180°C, which is well within the recommended range of the manufacturer. The shear rate used in the study were in the range 0.01–100 1/s, and air gap was 0.1 mm. The melting enthalpy and melting temperature were measured by differential scanning calorimetry (Diamond DSC, Perkin Elmer Inc., Shelton, Connecticut, U.S.). The DSC specimens (2 mg) were encapsulated in aluminum pans and treated at a heating rate of 10°C/min. The atmosphere was nitrogen with a flow rate of 45 mL/min. The analytical temperature range was set between 40°C and 200°C. Dynamic mechanical analysis (DMA) was performed using a DMA Q800 instrument (TA Instruments, New Castle, Delaware, U.S.). Measurements were

conducted over a temperature range of 0°C–125°C at a constant frequency of 1 Hz. The DMA samples, with dimensions of 35.0 × 10.0 × 3.0 mm, were tested in a three-point bending mode. The flexural tests were conducted using the ASTM D-790 standard procedure with Instron 5567 (Instron, Norwood, Massachusetts, U.S.). The dimensions of the flexural test specimens were 65 mm in length, 12.7 mm in width, 3.5 mm in thickness, 56 mm in span length, and a cross-head speed of 1.48 mm/min.

3 | Results and Discussion

3.1 | PA6-GNPs Resin Properties

The crystallization and melting behaviors of PA6-based resin with varying GNPs contents were systematically analyzed using DSC, as illustrated in Figure 2. Each sample displayed a singular endothermic peak, representative of the melting of the crystalline PA6 phase.

Figure 2a shows the DSC curves of pristine PA6 and GNPs-reinforced resins with GNPs contents of 0.3, 0.6, and 0.9 wt%. All samples exhibited a single endothermic peak corresponding to the melting of crystalline PA6, but the peak temperature and shape varied notably depending on GNPs loading. The pristine PA6 sample exhibited a sharp melting peak at 152.06°C, indicating the presence of a well-developed crystalline structure. In contrast, the 0.3 wt% GNPs composite showed a broader and less intense peak at a significantly lower temperature of 131.04°C, suggesting that the introduction of GNPs disrupted molecular chain alignment and reduced crystallinity [28]. The 0.6 wt% GNPs composite exhibited a melting peak at 145.93°C with a more pronounced shape, indicating that well-dispersed GNPs served as effective nucleating agents and facilitated more ordered and uniform crystallization [29]. On the other hand, the 0.9 wt% GNPs composite exhibited a flatter peak at 141.43°C, indicating that excessive GNPs loading led to agglomeration, which interfered with the regular growth of crystalline domains [30].

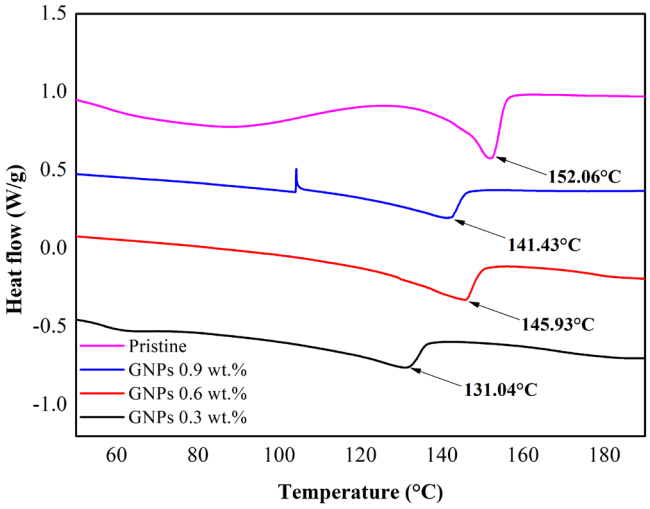

FIGURE 2 | (a) Differential scanning calorimetry (DSC) curves of pristine and GNPs-reinforced samples with varying GNPs contents of 0.3 wt%, 0.6 wt%, and 0.9 wt%.

Importantly, as shown in Figure 2b, while the melting temperature (Tm) of the GNPs-loaded samples slightly decreased compared with pristine PA6, the crystallinity calculated from the enthalpy of fusion increased with the addition of GNPs. This indicates that well-dispersed GNPs acted as effective nucleating agents, promoting ordered crystalline regions and enhancing structural integrity [31]. In other words, even though the overall onset of melting shifted to a lower temperature, the incorporation of GNPs resulted in improved crystallinity and interfacial stability, which can compensate for the reduction in Tm and contribute to mechanical reinforcement and dimensional stability under service conditions [28, 30].

Thus, the DSC analysis confirms that GNPs addition significantly influences the thermal characteristics of PA6 resin. A balanced loading of 0.6 wt% provided the most favorable outcome, showing improved crystallinity without severe agglomeration or loss of structural uniformity [29]. These findings support the role of GNPs as nucleating agents and highlight their potential to reinforce both the thermal and mechanical stability of PA6-based composites.

Figure 3 shows the shear viscosity of pristine PA6, film-based matrix, and GNPs-reinforced PA6 resin with 0.3, 0.6, and 0.9 wt% GNPs as a function of shear rate. All samples exhibited typical shear-thinning behavior, characterized by a decrease in viscosity with increasing shear rate. However, the overall viscosity levels and slope profiles varied depending on the matrix type and GNPs content. The film-based sample (Figure 3a) exhibited the highest viscosity at low shear rates, followed by a gradual decrease with increasing shear rate. This response is attributed to limited chain mobility during the melting of the solid PA6 film, along with the absence of effective molecular entanglement or network formation. The weak shear-thinning response is consistent with the poor matrix infiltration observed in morphological analysis, suggesting insufficient interfacial bonding and lack of structural continuity [31]. In comparison, the pristine PA6 resin (Figure 3b) exhibited lower viscosity and a more distinct shear-thinning curve, indicating a moderate degree of chain entanglement and improved molecular packing due to uniform matrix infiltration [32]. Among the GNPs-reinforced samples, GNPs 0.3 wt% resin (Figure 4c) showed the highest viscosity over the entire shear rate range (excluding film). This is likely due to increased polymer–filler interactions such as π–π stacking and van der Waals forces. However, the elevated viscosity may also reflect non-uniform GNPs dispersion or localized agglomeration, which hinders flow and elevates resistance [33]. GNPs 0.6 wt% resin (Figure 4d) exhibited a lower and more stable viscosity curve compared to the 0.3 and 0.9 wt% samples. The smooth shear-thinning trend suggests well-dispersed GNPs and formation of a uniform microstructural network, which suppresses polymer chain slippage and promotes consistent flow behavior [34]. GNPs 0.9 wt% resin (Figure 4e) showed moderate viscosity levels, but irregular fluctuations were observed at high shear rates. These instabilities are attributed to GNPs agglomeration at excessive filler content, leading to inconsistent chain mobility and rheological response [35]. In summary, the addition of GNPs significantly influenced the rheological properties of PA6-based resin. Although low GNPs content resulted in excessive viscosity due to localized interactions, high GNPs loading caused instability due to agglomeration. GNPs 0.6 wt% resin demonstrated the most favorable combination of dispersion

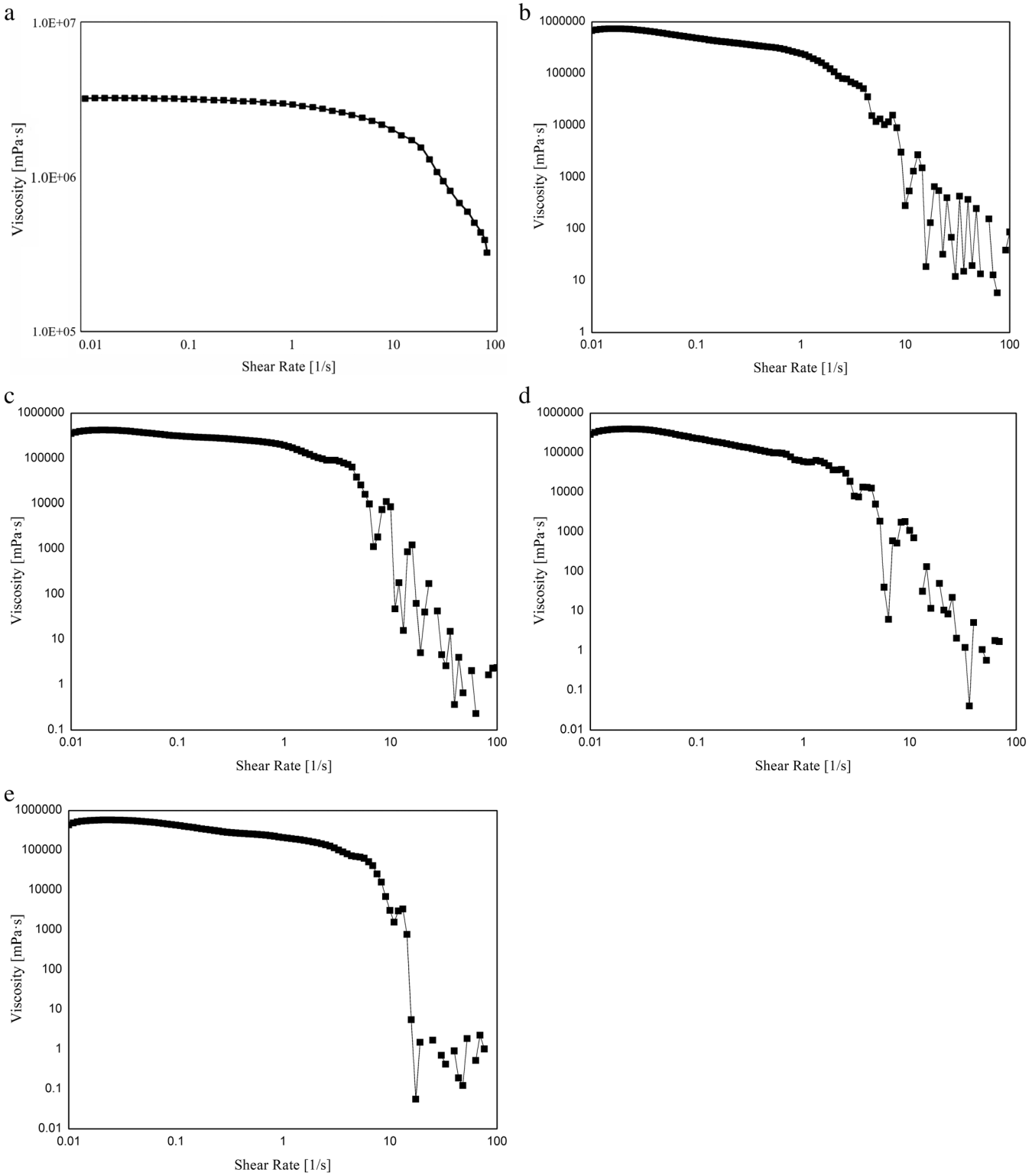

FIGURE 3 | Shear viscosity as a function of shear rate for various PA6-based samples. (a) Film-based matrix sample, (b) pristine PA6, (c) GNPs 0.3 wt%, (d) GNPs 0.6 wt%, and (e) GNPs 0.9 wt% resin.

quality, flow stability, and microstructural uniformity, making it the optimal composition in terms of processability and structural reliability.

Storage modulus (E′), loss modulus (E″), and damping factor (tan δ) were measured as functions of temperature. The DMA results in Figure 4 compare pristine PA6, PA6 reinforced with 0.3, 0.6, and 0.9 wt% GNPs, and the film-based specimen. In terms of storage stiffness, the film-based specimen exhibited the lowest response across the entire temperature range, consistent with insufficient resin impregnation and weak fiber–matrix adhesion; its initial (low-temperature) maximum E′ was 4605 MPa at 0.47°C. By contrast, pristine PA6 showed a markedly higher initial E′ of 14,209 MPa at 6.0°C (Figure 4b), indicative of

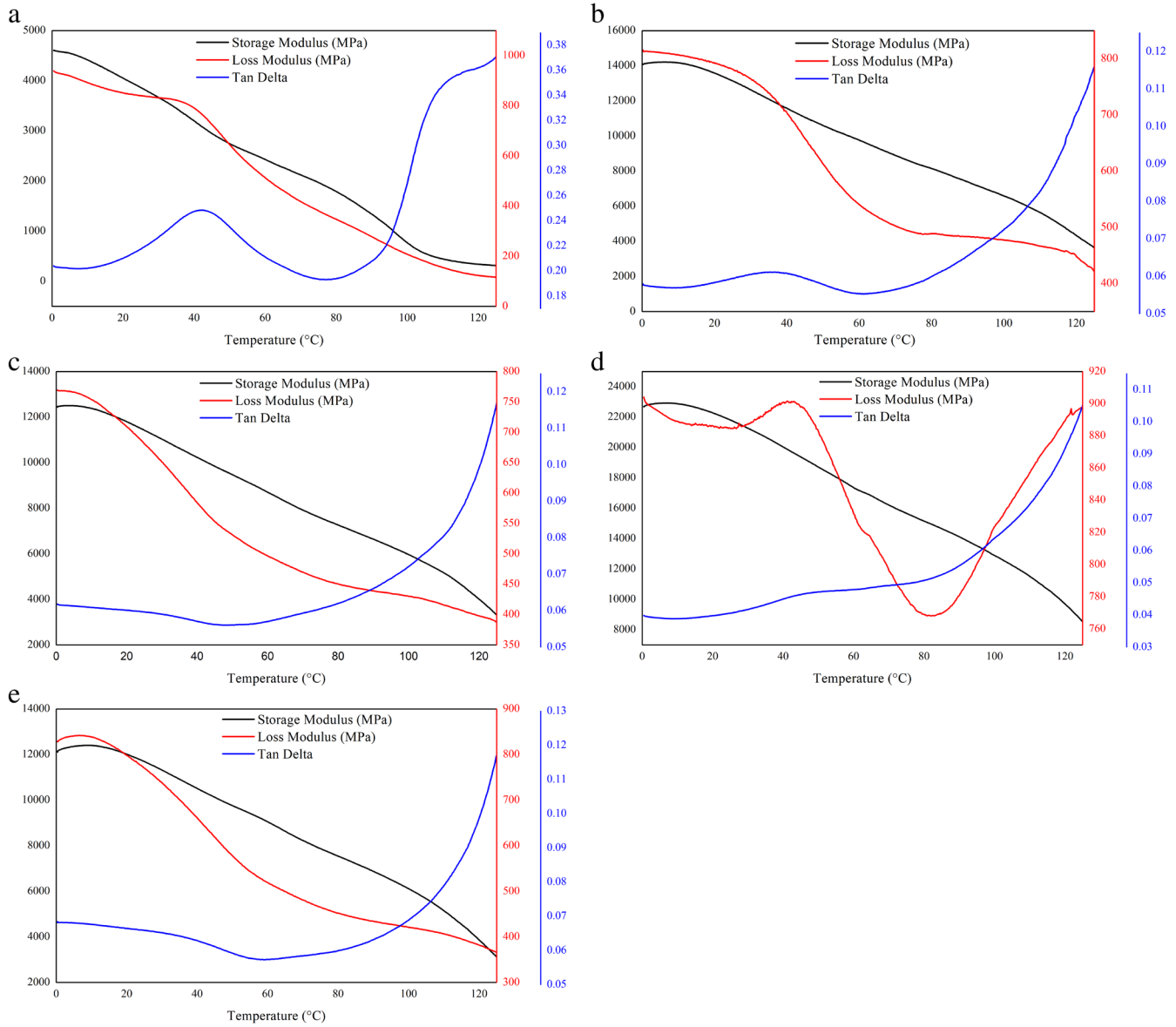

FIGURE 4 | Dynamic mechanical analysis (DMA) results of PA6-based resin with different GNPs contents and the film-based sample: (a) Film matrix, (b) Pristine PA6, (c) GNPs 0.3 wt%, (d) GNPs 0.6 wt%, and (e) GNPs 0.9 wt% resin.

effective solution-matrix infiltration and good structural integrity [36]. Adding 0.3 wt% GNPs yielded a modest increase (12,501 MPa at 3.6°C), whereas 0.6 wt% GNPs produced the most pronounced improvement (22,928 MPa at 7.0°C), consistent with a well-developed GNPs network that promotes load transfer and rigidity [37]. At 0.9 wt% GNPs, the initial E′ decreased to 12,405 MPa at 8.6°C, likely due to GNPs agglomeration that interrupts stress-transfer pathways [29].

The E″ curves reflect internal friction and the extent of chain restriction. The film-based specimen displayed sharp, localized dissipation with a main E″ peak at 38.42°C (804.1 MPa), in line with non-uniform chain mobility arising from incomplete impregnation. Pristine PA6 exhibited a broader, lower-intensity response with an E″ peak at 32.19°C (754.6 MPa), reflecting relatively free chain motion in the absence of reinforcing structures [36]. The 0.3 wt% GNPs resin showed a broad, featureless profile but with an early E″ peak at 11.53°C (748.7 MPa), suggesting uneven dispersion and only partial reinforcement. In contrast, 0.6 wt% GNPs produced a distinct E″ peak at 42.42°C (901.4 MPa), evidencing targeted energy dissipation and strong polymer–filler interactions within a uniform reinforcing network [38]. The 0.9 wt% GNPs resin exhibited a flatter, more irregular curve with a low-temperature E″ peak at 6.60°C (842.1 MPa), consistent with reduced reinforcing efficiency due to agglomeration [37, 39].

The glass transition temperature (T_g) was assigned from the most pronounced (dominant) peak of the tan δ curve (α-relaxation); minor low-temperature shoulders or secondary peaks were disregarded. Loss-modulus (E″) peaks were used solely for cross-validation, not for assigning T_g. Using this criterion, the tan δ peak temperatures/values (and T_g) were: film 42.30°C/0.2484 ($T_g = 42.30$°C); pristine 36.61°C/0.6112 ($T_g = 36.61$°C); 0.3 wt% GNPs: no resolvable dominant tan δ peak within the scanned range ($T_g = n.d.$); 0.6 wt% GNPs

43.18°C/0.4595 ($Tg = 43.18$°C); 0.9 wt% GNPs 56.99°C/0.05738 ($T_g = 56.99$°C) [34, 40]. Taken together, the 0.6 wt% GNPs resin achieves the most balanced combination of high initial E′, a strong and well-positioned E″ peak, and a moderate T_g, consistent with optimal dispersion and a stable reinforcing network. Lower loading yields limited reinforcement, whereas excessive loading leads to agglomeration and degraded performance [36, 37]. It should also be noted that the DMA measurements were intentionally limited to 120°C to ensure reliable bending-mode data. As confirmed by the DSC results (Figure 2), the melting endotherms of PA6-based resins appear in the range of 131°C–152°C. Approaching this region, the polymer matrix undergoes excessive softening and potential specimen slippage in the fixture, which can distort viscoelastic responses. Therefore, the DMA sweep was capped at 120°C to provide meaningful and comparable viscoelastic properties across all samples, while avoiding artifacts caused by matrix softening and flow.

3.2 | CFRPs Flexural Properties

The mechanical performance of PA6-based CFRPs containing 0.3, 0.6, and 0.9 wt% GNPs was evaluated through three-point bending tests, and the results are summarized in Figure 5a,b. Flexural stress–strain curves, flexural strength, flexural modulus were analyzed. As shown in Figure 5a, the flexural strengths of the Film, Pristine, GNPs 0.3 wt%, GNPs 0.6 wt%, and GNPs 0.9 wt% specimens were 61.20 ± 2.0 MPa, 342.18 ± 28 MPa, 393.71 ± 12 MPa, 436.58 ± 42 MPa, and 417.15 ± 58 MPa, respectively. The film-based sample exhibited the lowest flexural strength and modulus among all specimens. However, it showed the highest strain at break, as evidenced by its prolonged deformation at low stress levels in the stress–strain curve (Figure 5b). This behavior is attributed to the insufficient resin penetration into the carbon fiber bundles during compression molding, which led to poor fiber–matrix interfacial bonding and significantly reduced structural stiffness. The extended deformation, despite low strength, suggests that viscous dissipation and fiber–fiber friction dominated the mechanical response rather than elastic load-bearing, a characteristic of poorly bonded composites [41]. The pristine PA6 specimen exhibited a maximum flexural strength of approximately 342 MPa, reflecting the typical mechanical behavior of a semi-crystalline thermoplastic composite with balanced structural integrity and moderate ductility [42]. GNPs 0.3 wt% composite increased strength, reaching a flexural strength of 393.71 ± 12 MPa. However, strain at break slightly decreased, indicating that filler–matrix interfacial interactions restricted chain mobility [43]. GNPs 0.6 wt% composite showed the most favorable mechanical performance. As presented in Figure 5a,b, this sample achieved the highest flexural strength (436.58 ± 42 MPa), and a moderately high strain at break of 3.1%. This indicates the formation of a continuous and well-dispersed GNPs reinforcement network, which enhanced stress transfer and mechanical rigidity [44]. In contrast, GNPs 0.9 wt% composite exhibited a slight decrease in strength (417.15 ± 58 MPa) and strain at break (2.9%) compared to the 0.6 wt% sample. This deterioration is attributed to GNPs agglomeration at excessive loadings, which disrupted the continuity of the reinforcing network and induced localized stress concentrations, leading to premature brittle fracture [29, 45]. In summary, the flexural performance of PA6 composites was significantly influenced by both the GNPs content and dispersion quality. GNPs 0.6 wt% composite demonstrated the best overall mechanical response by achieving an optimal balance between stiffness and ductility. In contrast, both underfilled (0.3 wt%) and overfilled (0.9 wt%) composites showed inferior properties due to insufficient network formation or filler agglomeration, respectively [46, 47]. Although the film-based sample exhibited the highest elongation, its poor resin infiltration and lack of structural continuity led to the lowest flexural strength. These results underscore the importance of optimizing both GNPs loading and dispersion for maximizing the reinforcing effect in PA6-based nanocomposites.

Figure 6 presents the optical micrographs of the cross-sectional morphologies of CFRPs fabricated using various matrix types and GNPs contents. Sample (a) represents conventional epoxy-based CFRPs, (b) corresponds to the PA6 film-based matrix, (c) is the pristine PA6 solution-based composite, and (d–f) are

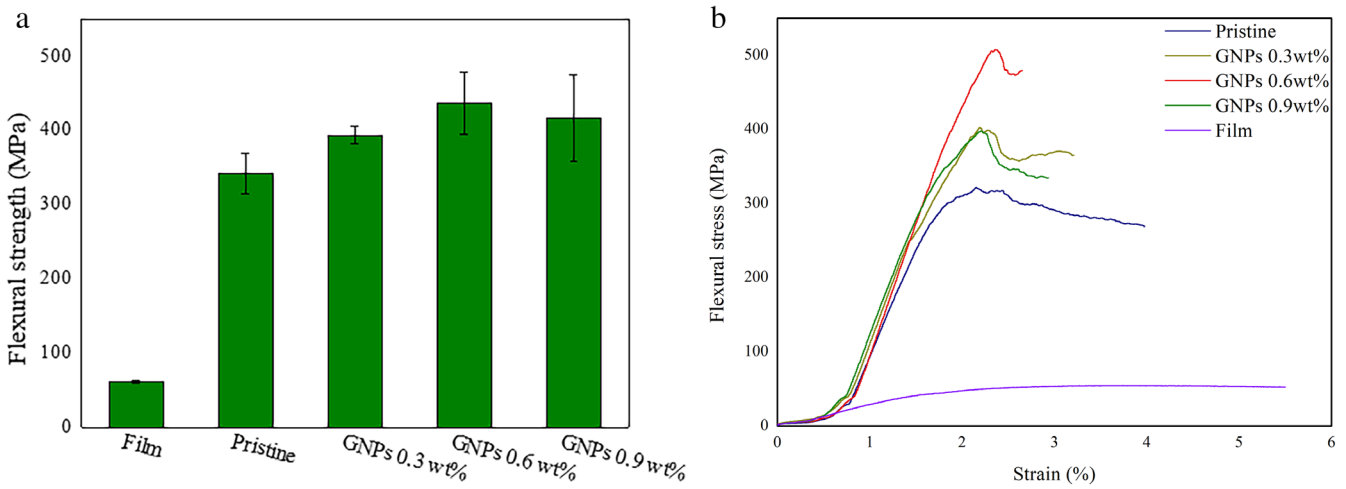

FIGURE 5 | Flexural behavior of PA6-based composites reinforced with various GNPs contents: (a) flexural strength values for each CFRP with various contents of GNPs, (b) flexural stress–strain curves.

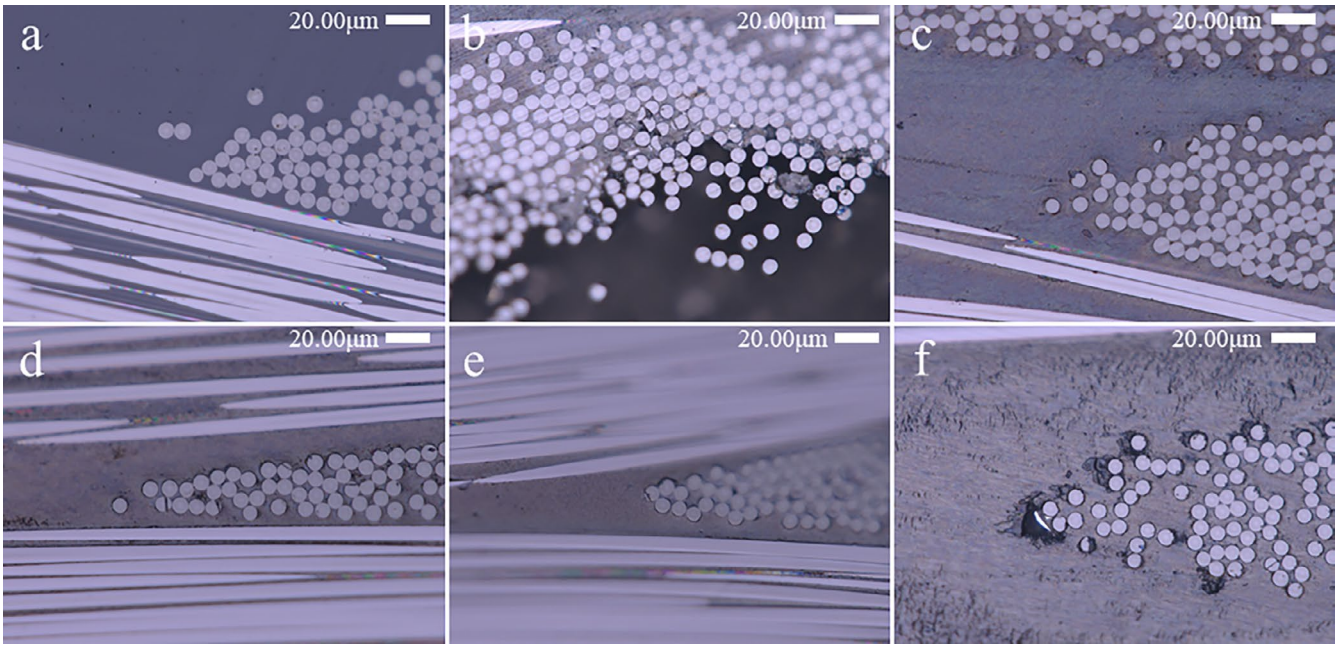

FIGURE 6 | Optical micrographs of cross-sectional morphologies of carbon fiber reinforced thermoplastic composites fabricated with different matrix types and GNPs contents: (a) CFRPs with epoxy matrix, (b) CFRPs with polyamide film matrix (film), (c) Pristine, (d–f) GNPs-reinforced PA6 composites with 0.3, 0.6, and 0.9 wt% GNPs, respectively.

composites with 0.3, 0.6, and 0.9 wt% GNPs, respectively. In the epoxy-based sample (Figure 6a), the matrix was observed to be uniformly infiltrated between the carbon fiber bundles, and no significant voids or fiber pull-out regions were found. This is consistent with the well-established impregnation characteristics of low-viscosity thermoset epoxy resins, which enable strong interfacial adhesion and dense composite structures [44]. In contrast, the PA6 film-based sample (Figure 6b) exhibited poor matrix infiltration, with large interstitial voids and incomplete matrix coverage between fiber bundles. The solid-state PA6 film likely failed to sufficiently infiltrate the interior of the carbon fiber bundles during compression molding, resulting in inadequate mechanical interlocking and extensive void formation. This morphological evidence is in agreement with the poor mechanical performance shown in flexural tests for the film-based composite. The pristine sample (Figure 6c) exhibited uniform matrix infiltration into the fiber network with relatively low void content. This suggests that the solution-based matrix effectively infiltrated the spaces between fibers, and that solidification during compression resulted in strong structural integration. The GNPs-reinforced samples (d–f) showed morphology changes depending on GNPs content. The GNPs 0.3 wt% composite (Figure 6d) demonstrated similar infiltration and matrix distribution to the pristine sample, with no signs of agglomeration. The GNPs 0.6 wt% composite (Figure 6e) displayed the most uniform and compact matrix distribution among the fiber bundles, indicating well-dispersed GNPs and the formation of an optimal reinforcing network. In contrast, the GNPs 0.9 wt% composite (Figure 6f) exhibited some micro-voids, which are likely the result of poor GNPs dispersion and hindered flow during molding [42]. These morphological observations are directly correlated with the flexural results shown in Figure 5. In particular, the 0.6 wt% GNPs composite exhibited the most uniform resin infiltration and minimal void content (Figure 6e), which enabled efficient stress transfer between fibers and matrix, thereby explaining its superior flexural performance. Conversely, the poor infiltration in the film-based sample and the micro-voids in the 0.9 wt% GNPs composite are consistent with their lower flexural strength and reduced reliability. The dispersion quality of GNPs therefore plays a critical role in determining matrix infiltration and void formation. Taken together, these findings clarify that the superior flexural performance of the 0.6 wt% GNPs composite is attributed to its most favorable interfacial contact and structural integration [48].

4 | Conclusions

In this study, materials suitable for next-generation hydrogen storage vessel structures were explored through the evaluation of the properties of graphene-enhanced PA6 resin and carbon fiber-reinforced composites. Using this enhanced resin, we fabricated composites that exhibited clear improvements in flexural modulus and flexural strength. Thermal analysis further revealed that the addition of GNPs slightly reduced the melting temperature but increased the crystallinity, confirming the role of GNPs as effective nucleating agents that promote ordered crystalline growth. The optimal GNPs content was identified as 0.6 wt%, which provided the best balance of crystallinity, flexural strength (≈437 MPa), and modulus under the processing conditions. These improvements were directly correlated with uniform resin infiltration and reduced void formation, enabling efficient stress transfer between fiber and matrix and thereby explaining the superior flexural performance of the 0.6 wt% composite. Taken together, these findings indicate that GNPs modification is an effective strategy to simultaneously improve the thermal behavior, mechanical reinforcement, and structural reliability of PA6-based composites, supporting their application

in Type IV hydrogen storage vessels and suggesting potential for future Type V vessels.

Author Contributions

Jonghyun Eun: conceptualization, writing – original draft. **Sun-Woo Kang:** validation, formal analysis, methodology, conceptualization. **Myeongjin Park:** validation, visualization. **Joon Seok Lee:** supervision, project administration, funding acquisition. **Hyunchul Ahn:** supervision, writing – review and editing, project administration.

Acknowledgments

This study was supported by the Technology Innovation Program (20011899) funded by the Ministry of Trade, Industry & Energy (MOTIE, Korea) and supported by the 2023 Yeungnam University Research Grant.

Conflicts of Interest

The authors declare no conflicts of interest.

Data Availability Statement

The data that support the findings of this study are available from the corresponding author upon reasonable request.

References

1. N. Kumar, S. Y. Lee, and S. J. Park, "Advancements in Hydrogen Storage Technologies: A Comprehensive Review of Materials, Methods, and Economic Policy," *Nano Today* 56 (2024): 102302.

2. E. Rivard, M. Trudeau, and K. Zaghib, "Hydrogen Storage for Mobility: A Review," *Materials* 12, no. 12 (2019): 1973.

3. P. Chen and M. Zhu, "Recent Progress in Hydrogen Storage," *Materials Today* 11, no. 12 (2008): 36–43.

4. Y. Yan, J. Zhang, G. Li, et al., "Review on Linerless Type V Cryo-Compressed Hydrogen Storage Vessels: Resin Toughening and Hydrogen-Barrier Properties Control," *Renewable and Sustainable Energy Reviews* 189 (2024): 114009.

5. I. Feki, M. Shirinbayan, S. Nouira, et al., "Multi-Scale Fatigue Damage Analysis in Filament-Wound Carbon Fiber Reinforced Epoxy Composites for Hydrogen Storage Tanks," *Composites Part C: Open Access* 15 (2024): 100537.

6. Z. Zhang, Q. Ji, Z. Guo, et al., "Design, Preparation, and Mechanical Properties of Glass Fiber Reinforced Thermoplastic Self-Anchor Plate Cable Exposed in Alkaline Solution," *Polymer Composites* 45, no. 13 (2024): 11687–11700.

7. C. Dong, Y. Liu, J. Li, et al., "Hydrogen Permeability of Polyamide 6 Used as Liner Material for Type Iv On-Board Hydrogen Storage Cylinders," *Polymers* 15 (2023): 3715.

8. Y. Su, H. Lv, C. Feng, et al., "Hydrogen Permeability of Polyamide 6 as the Liner Material of Type IV Hydrogen Storage Tanks: A Molecular Dynamics Investigation," *International Journal of Hydrogen Energy* 50 (2024): 1598–1606.

9. L. Wang, B. Wang, S. Wei, Y. Hong, and C. Zheng, "Prediction of Long-Term Fatigue Life of CFRP Composite Hydrogen Storage Vessel Based on Micromechanics of Failure," *Composites Part B: Engineering* 97 (2016): 274–281.

10. C. Li and G. Xian, "Mechanical Property Evolution and Life Prediction of Carbon Fiber and Pultruded Carbon Fiber Reinforced Polymer Plate Exposed to Elevated Temperatures," *Polymer Composites* 41 (2020): 5143–5155.

11. Y. Sun, H. Lv, W. Zhou, et al., "Research on Hydrogen Permeability of Polyamide 6 as the Liner Material for Type IV Hydrogen Storage Tank," *International Journal of Hydrogen Energy* 45 (2020): 24980–24990.

12. H. T. Hwang and A. Varma, "Hydrogen Storage for Fuel Cell Vehicles," *Current Opinion in Chemical Engineering* 5 (2014): 42–48.

13. A. Kausar, "Composite Coatings of Polyamide/Graphene: Microstructure, Mechanical, Thermal, and Barrier Properties," *Composite Interfaces* 25 (2018): 109–125.

14. K. Bilisik and M. Akter, "Polymer Nanocomposites Based on Graphite Nanoplatelets (GNPs): A Review on Thermal-Electrical Conductivity, Mechanical and Barrier Properties," *Journal of Materials Science* 57 (2022): 7425–7480.

15. M. Sabet and H. Soleimani, "The Influence of Graphene on the Mechanical, Thermal, and Flame Retardant Characteristics of Polyamide 6," *Materials Technology* 37 (2022): 1251–1262.

16. M. Nachtane, M. Tarfaoui, M. A. Abichou, et al., "An Overview of the Recent Advances in Composite Materials and Artificial Intelligence for Hydrogen Storage Vessels Design," *Journal of Composites Science* 7 (2023): 119.

17. H. V. Madhad and D. V. Vasava, "Review on Recent Progress in Synthesis of Graphene–Polyamide Nanocomposites," *Journal of Thermoplastic Composite Materials* 35 (2019): 570–598.

18. A. Zhang, R. Liu, J. Tian, W. Huang, and J. Liu, "MXene-Based Nanocomposites for Energy Conversion and Storage Applications," *Chemistry—a European Journal* 26 (2020): 6342–6359.

19. A. Uthaman, H. M. Lal, C. Li, G. Xian, and S. Thomas, "Mechanical and Water Uptake Properties of Epoxy Nanocomposites With Surfactant-Modified Functionalized Multiwalled Carbon Nanotubes," *Nanomaterials* 11 (2021): 1234.

20. D. E. Abulyazied and A. Ene, "An Investigative Study on the Progress of Nanoclay-Reinforced Polymers: Preparation, Properties, and Applications: A Review," *Polymers* 13 (2021): 4401.

21. H. Sepetcioglu, "Experimental Study on the Effect of Graphene Nanoplatelets on the Low-Velocity Impact Response of Prestressed Filament Wound Basalt-Based Composite Pressure Vessels," *Polymer Composites* 42, no. 10 (2021): 5527–5540.

22. H. Sepetcioglu, N. Tarakcioglu, and R. Rafiee, "Experimental Investigation of Graphene Nanoplatelets Effect on the Fatigue Behavior of Basalt/Epoxy Composite Pressure Vessels," *Thin-Walled Structures* 171 (2022): 108672.

23. H. Sepetcioglu and N. Tarakcioglu, "Fatigue Behavior of Graphene Nanoplatelets Reinforced and Unreinforced Basalt/Epoxy Composite Pressure Vessels Subjected to Low-Velocity Impact Under Internal Pressure," *Journal of Composite Materials* 55, no. 29 (2021): 4361–4373.

24. H. Sepetcioglu and N. Tarakcioglu, "Effect of Graphene Nanoplatelets on Progressive Failure Behavior Under Internal Pressure of Composite Cylindrical Pressure Vessels," *Journal of Materials Engineering and Performance* 31 (2022): 2225–2239.

25. H. Sepetcioglu, L. Lapčík, B. Lapčíková, et al., "Improved Mechanical Properties of Graphene-Modified Basalt Fibre–Epoxy Composites," *Nanotechnology Reviews* 13 (2024): 20240052.

26. D. Guillon, D. Espinassou, P. Pichon, et al., "Manufacturing, Burst Test and Modeling of High Pressure Thermoplastic Composite Overwrap Pressure Vessel," *Composite Structures* 316 (2023): 116965.

27. J. Eun, D. Kim, H. Ahn, et al., "Compatibility of Liner Materials for Type IV Hydrogen Storage Vessels and the Interlaminar Properties of Liner/CFRP Composites," *International Journal of Hydrogen Energy* 133 (2025): 431–439.

28. J. Lagarinhos, S. M. da Silva, and J. M. Oliveira, "Non-Isothermal Crystallization Kinetics of Polyamide 6/Graphene Nanoplatelets

Nanocomposites Obtained via In Situ Polymerization: Effect of Nanofiller Size," *Polymers* 15 (2023): 4109.

29. X. Yao, T. Raine, M. Liu, et al., "Effect of Graphene Nanoplatelets on the Mechanical and Gas Barrier Properties of Woven Carbon Fibre/Epoxy Composites," *Journal of Materials Science* 56 (2021): 19538–19551.

30. E. Tarani, I. Arvanitidis, D. Christofilos, D. N. Bikiaris, K. Chrissafis, and G. Vourlias, "Calculation of the Degree of Crystallinity of HDPE/GNPs Nanocomposites by Using Various Experimental Techniques: A Comparative Study," *Journal of Materials Science* 58 (2023): 1621–1639.

31. W. Meng and K. Khayat, "Effect of Graphite Nanoplatelets and Carbon Nanofibers on Rheology, Hydration, Shrinkage, Mechanical Properties, and Microstructure of UHPC," *Cement and Concrete Research* 105 (2018): 64–71.

32. Z. Su, Z. Wang, D. Zhang, and T. Wei, "Study on Rheological Behavior and Surface Properties of Epoxy Resin Chemical Grouting Material Considering Time Variation," *Materials* 12 (2019): 3277.

33. R. Atif, I. Shyha, and F. Inam, "Mechanical, Thermal, and Electrical Properties of Graphene-Epoxy Nanocomposites-A Review," *Polymers* 8 (2016): 281.

34. A. Oun, A. Manalo, O. Alajarmeh, R. Abousnina, and A. Gerdes, "Influence of Elevated Temperature on the Mechanical Properties of Hybrid Flax-Fiber–Epoxy Composites Incorporating Graphene," *Polymers* 14 (2022): 1841.

35. M. Weir, D. Johnson, S. Boothroyd, et al., "Distortion of Chain Conformation and Reduced Entanglement in Polymer-Graphene Oxide Nanocomposites," *ACS Macro Letters* 5 (2016): 430–434.

36. W. Goertzen and M. Kessler, "Dynamic Mechanical Analysis of Carbon/Epoxy Composites for Structural Pipeline Repair," *Composites Part B: Engineering* 38 (2007): 1–9.

37. C. M. Hadden, D. R. Klimek-Mcdonald, E. J. Pineda, et al., "Mechanical Properties of Graphene Nanoplatelet/Carbon Fiber/Epoxy Hybrid Composites: Multiscale Modeling and Experiments," *Carbon* 95 (2015): 100–112.

38. A. Durmuş-Sayar, M. Tansan, T. Çinko-Çoban, et al., "Incorporation of Graphene Nanoplatelets Into Fiber-Reinforced Polymer Composites in the Presence of Highly Branched Waterborne Polyurethanes," *Polymers* 16 (2024): 828.

39. G. Sherif, D. Chukov, V. Tcherdyntsev, and V. Torokhov, "Effect of Formation Route on the Mechanical Properties of the Polyethersulfone Composites Reinforced With Glass Fibers," *Polymers* 11 (2019): 1364.

40. H. Kaftelen-Odabaşı, A. Odabaşı, M. Özdemir, and M. Baydoğan, "A Study on Graphene Reinforced Carbon Fiber Epoxy Composites: Investigation of Electrical, Flexural, and Dynamic Mechanical Properties," *Polymer Composites* 44 (2023): 121–135.

41. J. Misumi and T. Oyama, "Low Viscosity and High Toughness Epoxy Resin Modified by In Situ Radical Polymerization Method for Improving Mechanical Properties of Carbon Fiber Reinforced Plastics," *Polymer* 156 (2018): 1–9.

42. M. Pawlik, H. Le, and Y. Lu, "Effects of the Graphene Nanoplatelets Reinforced Interphase on Mechanical Properties of Carbon Fibre Reinforced Polymer—A Multiscale Modelling Study," *Composites Part B Engineering* 177 (2019): 107097.

43. M. Dong, Y. Sun, D. Dunstan, D. J. Dunstan, R. J. Young, and D. G. Papageorgiou, "Mechanical Reinforcement From Two-Dimensional Nanofillers: Model, Bulk and Hybrid Polymer Nanocomposites," *Nanoscale* 16 (2024): 13247–13299.

44. S. Lee, S. Yoon, and I. Jeon, "Graphene/Polymer Nanocomposites: Preparation, Mechanical Properties, and Application," *Polymers* 14 (2022): 4733.

45. R. Gupta, G. Kumar, H. Bisaria, and S. Zafar, "Effect of Graphene Nanoparticles on Electrical, Mechanical and Viscoelastic Behavior of CFRP Multifunctional Multiscale Composites," *Polymer Composites* 46 (2024): 6885–6899.

46. B. Abhiram and D. Ghosh, "Influence of Nanofiller Agglomeration on Fracture Properties of Polymer Nanocomposite: Insights From Atomistic Simulation," *Engineering Fracture Mechanics* 290 (2023): 109503.

47. R. Suresha, H. Sachidananda, B. Shivamurthy, H. K. Sachidananda, N. K. Swamy, and S. Parasuram, "Mechanical and Electromagnetic Shielding Properties of Carbon Fabric With Graphene Nanoplatelets Reinforced Epoxy Composites," *Scientific Reports* 15 (2025): 15735.

48. J. Ubaid, J. Andrew, W. Cantwell, et al., "Performance Evaluation of GNP-Modified Epoxy/Carbon Fiber Composites After Cryogenic Thermal Cycling for Hydrogen Storage Applications," *International Journal of Hydrogen Energy* 159 (2025): 150574.